Electron–phonon interactions in $CsCdBr_3:Yb^{3+}$

Markus P. Hehlen, Amos Kuditcher, and Stephen C. Rand
Optical Sciences, The University of Michigan, Ann Arbor, Michigan 48109-2122

Michael A. Tischler
The Harrison M. Randall Laboratory of Physics, The University of Michigan, Ann Arbor, Michigan 48109-1120

(Received 11 June 1997; accepted 24 June 1997)

Pronounced electron–phonon coupling is observed for the $^2F_{7/2} \leftrightarrow {}^2F_{5/2}$ $4f$ transitions of Yb^{3+} doped into $CsCdBr_3$. A comparison of the Raman spectrum and the luminescence excitation sideband accompanying the $^2F_{7/2}(0) \rightarrow {}^2F_{5/2}(2')$ crystal-field transition reveals vibrational properties of the $[YbBr_6]$ coordination unit that differ markedly from those of the $CsCdBr_3$ host. In particular, the vibronic transition associated with the totally symmetric $[YbBr_6]$ stretching mode appears as a very weak feature at 191 cm^{-1} in the Raman spectrum, whereas the totally symmetric $[CdBr_6]$ stretching mode of the $CsCdBr_3$ bulk, which appears as a strong feature at 162.5 cm^{-1} in the Raman spectrum, is only weakly discernible in the sideband. This is direct evidence for a large contribution from $[YbBr_6]$ local modes and a small contribution from bulk modes to the vibronic intensity. The intensity of the local mode is enhanced by approximately a factor of 2 in the Raman spectrum when the laser is tuned into resonance with the $^2F_{7/2}(0) \rightarrow {}^2F_{5/2}(2')$ absorption of Yb^{3+}, providing direct confirmation of its assignment. The observation of the first and second members of a Franck–Condon progression for both the local and the bulk totally symmetric modes indicates that a Δ process, rather than an M process, induces the vibronic intensity. Huang–Rhys factors of $S_{\text{local}} = 0.010 \pm 0.002$ and $S_{\text{bulk}} = 0.15 \pm 0.03$ were determined from the data, and reflect quite different electron–phonon coupling strengths. These results suggest that multiphonon relaxation of excited electronic states proceeds by the excitation of local modes of $[YbBr_6]$ followed by energy transfer to bulk modes of the lattice, possibly through a nonlinear coupling mechanism which is discussed briefly. © *1997 American Institute of Physics.* [S0021-9606(97)00637-5]

I. INTRODUCTION

The optical spectra of noncentrosymmetric solids doped with trivalent rare-earth (RE^{3+}) ions typically are dominated by electric-dipole induced electronic transitions between the states of the $4f$ shell. These electronic transitions can be accompanied by vibronic sidebands which are a result of interactions of the $4f$ electronic system with the various vibrational modes of the surroundings of the RE^{3+} ion. With the exception of Pm^{3+}, vibronic sidebands have been observed for all the RE^{3+} ions in a variety of solids.[1–4] The integrated intensity of the vibronic sideband relative to its zero-phonon line is usually low, although vibronic transition probabilities approaching or even exceeding zero-phonon transition probabilities have been found for certain transitions in some compounds.[5–8] Recently, Gd^{3+} and Pr^{3+}-doped crystals received particular attention for, besides having advantageous energy levels, they represent the extrema of the unexplained minimum of the electron–phonon–coupling strength in the middle of the lanthanide series.[9]

Vibronic sidebands, although usually weak and often ignored, are just one of the many manifestations of electron–phonon coupling in rare-earth-ion doped solids. Multiphonon relaxation of excited states and phonon-assistance in nonresonant energy transfer are other ubiquitous phenomena of key importance to excited-state dynamics and, ultimately, to the role rare-earth ions play in their many applications. Knowledge of the electron–phonon coupling strength as well as the spatial extension of the electron–phonon interaction is therefore a prerequisite to a detailed understanding of the energy flow in electronic dynamics involving the vibrational system. Direct information on the spatial extension of electron–phonon interactions in particular is difficult to obtain, since in most luminescent materials such as RE^{3+}-doped YAG, $YLiF_4$, $LaCl_3$, or $Cs_3Lu_2Br_9$, in which the RE^{3+} ion substitutes for a chemically similar ion, the vibrational properties of the nearest surroundings of the RE^{3+} ion are almost identical to those of the host lattice. One exception is the class of compounds containing well-defined molecular species. The ternary chloride $(NH_4)_2GdCl_5$ for example contains NH_4^+ molecular units in the second coordination sphere of Gd^{3+}, and electron–phonon coupling beyond the first $[GdCl_6]$ coordination sphere to NH_4^+ vibrational modes was observed in the $^6P_{7/2} \rightarrow {}^8S$ luminescence sideband.[10] In $(NH_4)_3YCl_6:Eu^{3+}$, electron–phonon coupling to those high frequency NH_4^+ vibrational modes in the second coordination sphere was suggested to account for the unusually low Eu^{3+} luminescence quantum yield of this material.[10] Rare-earth-ion doped compounds such as CaF_2, CdF_2, $CsMgCl_3$, or $CsCdBr_3$, in which RE^{3+} ions substitute for divalent metal ions, constitute another class of materials for which electron–phonon coupling beyond the first coordination sphere may be directly observed. Various defect structures are formed in these materials as a result of charge compensation. These defects typically have different symmetry

 0021-9606/97/107(13)/4886/7/$10.00

properties which, in addition to the different mass and charge of the RE^{3+} ion, may significantly alter the vibrational properties compared to the respective host lattice site. In this context, the vibrational system may be regarded as being composed of the local vibrational modes of the RE^{3+} defect embedded in the bulk modes of the host lattice.

In this paper we present a detailed study of vibronic coupling in Yb^{3+}-doped $CsCdBr_3$. The comparison of the Raman spectrum with the luminescence excitation spectrum of the sideband accompanying the ${}^2F_{7/2}(0)\rightarrow{}^2F_{5/2}(2')$ crystal-field transition of Yb^{3+} reveals strong coupling to the vibrational modes of the first Yb^{3+} coordination sphere and weak contributions from coupling to modes of the second coordination sphere and beyond. In particular, resonant Raman spectra are used to assign a weak feature in the Raman spectrum to the local mode associated with the highest-energy vibration of the first Yb^{3+} coordination sphere. The appearance of two-phonon replica of both the local and the bulk mode as well as of the respective combination mode in the vibronic sideband is direct evidence for a Franck–Condon-type process inducing the vibronic intensity. The results provide insight into the spatial extension of vibronic interactions and to the various steps required for the nonradiative relaxation of electronic excited states of rare-earth ions in solids.

II. EXPERIMENT

Optical quality crystals of Yb^{3+}-doped $CsCdBr_3$ were grown using the Bridgman technique from 99.5% cationic purity (c.p.) CsBr (dried in vacuum at 250 °C) and $CdBr_2$ (obtained from 99.998% c.p. CdO and HBr, and sublimed at 440 °C), and $YbBr_3$. The anhydrous $YbBr_3$ was obtained in a four-step process by formation of $(NH_4)_3YbBr_6$ from evaporating a 47% HBr solution of Yb_2O_3 (99.999% c.p.) and NH_4Br (99.8% c.p.), then drying of $(NH_4)_3YbBr_6$ in a nitrogen stream at 200 °C, decomposition of $(NH_4)_3YbBr_6$ to NH_4Br and $YbBr_3$ at 420 °C in vacuum,[11] and final sublimation of $YbBr_3$ at 1040 °C in a boron–nitride ampoule. The $CsCdBr_3$:Yb^{3+} sample was obtained from cutting a crystal along planes containing the crystallographic c-axis and applying an optical polish to the surfaces. The total ytterbium concentration of the sample used for this study was 1.47 ± 0.04 mol% as determined by inductively coupled plasma optical emission spectroscopy (ICP-OES). Since Yb^{3+} is easily reduced to Yb^{2+} and moreover, Yb substitutes for Cd^{2+} when doped into $CsCdBr_3$, typically both Yb^{3+} and Yb^{2+} will be present in a Yb-doped $CsCdBr_3$ crystal grown by the method described above. The yellow color of the crystal is indication for the presence of some Yb^{2+}, and therefore the Yb^{3+} concentration is likely to be smaller than the above value.

Polarized absorption spectra were recorded on a double-beam spectrophotometer with the sample cooled to 19 K by a closed-cycle helium refrigerator. An argon-ion laser pumped Ti:sapphire laser was used as excitation source for the near-infrared luminescence and luminescence excitation spectra. The sample luminescence was dispersed by a 1 m single monochromator and detected by a cooled InGaAs diode using a lock-in amplifier. The unpolarized Raman spectra were obtained using the polarization-scrambled 488.0 or 514.5 nm line of an argon-ion laser. The Raman spectrum was independent on the choice of either one of these wavelengths. The scattered light was collected in a backscattering arrangement, dispersed by a 1 m double monochromator, and detected by a photomultiplier and a photon counter. Unpolarized resonant Raman spectra were recorded using an argon-ion-laser pumped Ti:sapphire laser as excitation source in a similar geometry and with the sample cooled to 12 K by a closed-cycle helium refrigerator. The scattered light was dispersed by a triple monochromator and detected by a liquid-nitrogen-cooled CCD detector.

Except for the absorption and the resonant Raman spectra, all experiments were carried out at either 78.5 or 15.5 K with the sample mounted in a cold-finger cryostat.

III. RESULTS AND DISCUSSION

A. 4*f* energy levels of Yb^{3+} in $CsCdBr_3$

The diamagnetic salt $CsCdBr_3$ is a member of the inverse perovskite family with the hexagonal $CsNiCl_3$ structure.[12] It crystallizes in the D_{6h}^4 space group and consists of linear chains of face-sharing $[CdBr_6]^{4-}$ units with the chains being arranged along the crystallographic c-axis and the Cs^+ ions occupying high-symmetry sites between the chains. It was first shown by electron paramagnetic resonance (EPR) measurements that trivalent rare-earth ions (RE^{3+}) preferentially are incorporated as charge compensated RE^{3+}-vacancy-RE^{3+} ion pairs[13,14] having a RE^{3+}–RE^{3+} intra ion-pair distance of approximately 6.0 Å.[14] Several other RE^{3+} minority sites have since been identified. The point symmetry for a RE^{3+} ion on a Cd^{2+} site is C_{3v} (Refs. 15–19) thus, for odd $4f$-electron systems, the ${}^{2S+1}L_J$ multiplets are split into $(2J+1)/2$ Kramers doublets.

In its $[Xe]4f^{13}$ electron configuration, Yb^{3+} only has two multiplets, i.e., an ${}^2F_{7/2}$ ground state and an ${}^2F_{5/2}$ excited state which, in C_{3v} symmetry, are split into 4 and 3 crystal-field levels labeled (0), (1), (2), (3) and (0′), (1′), (2′), respectively. The three prominent lines observed at 10 122, 10 138, and 10 599 cm^{-1} in the 19 K absorption spectrum (Fig. 1) can consequently be assigned to the $(0)\rightarrow(0',1',2')$ zero-phonon transitions of Yb^{3+}, respectively. Each of the transitions is accompanied by a multipeak sideband which results from electron–phonon interactions discussed in Secs. III B and III C. The $(0)\rightarrow(0',1',2')$ energies are very similar to those measured in $Cs_3Yb_2Br_9$ (10 119, 10 146, 10 590 cm^{-1}, respectively[20]) in which Yb^{3+} has a sixfold bromide coordination geometry closely resembling the one of Yb^{3+} in $CsCdBr_3$:Yb^{3+}. From the luminescence spectrum (Fig. 2), the $(0')\rightarrow(0,1,2,3)$ transitions are found at 10 122, 10 007, 9 955, and 9 658 cm^{-1}, along with the $(1')\rightarrow(0,1,2,3)$ transitions which are observed as a result of thermal population of (1′) at 15.5 K. These energies indicate a ground-state splitting of 0, 115, 167, and 464 cm^{-1} which again is quite similar to that found in $Cs_3Yb_2Br_9$ [0, 114, 140, 441 cm^{-1} (Ref. 20).] Both the ground and excited-state

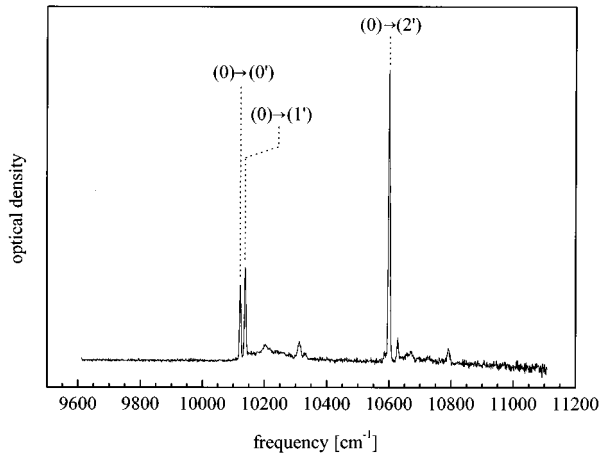

FIG. 1. Unpolarized $^2F_{7/2} \rightarrow {}^2F_{5/2}$ absorption spectrum of $CsCdBr_3:Yb^{3+}$ at 19 K. The labels (0) and $(0',1',2')$ refer to the crystal-field levels of the $^2F_{7/2}$ ground state and $^2F_{5/2}$ excited-state multiplet, respectively.

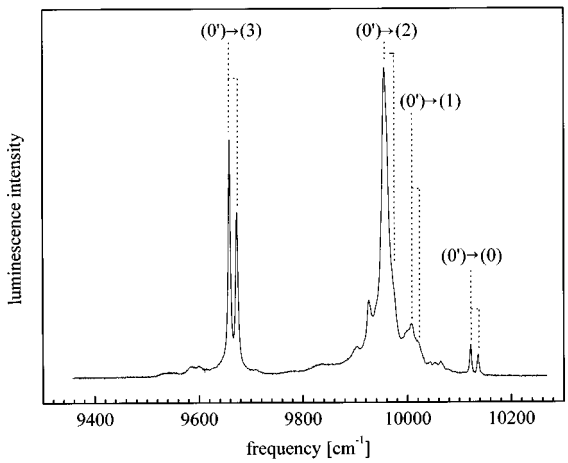

FIG. 2. Unpolarized $^2F_{5/2} \rightarrow {}^2F_{7/2}$ luminescence spectrum of $CsCdBr_3:Yb^{3+}$ at 15.5 K. The labels (0,1,2,3) and $(0',1')$ refer to the crystal-field levels of the $^2F_{7/2}$ ground state and $^2F_{5/2}$ excited-state multiplet, respectively.

splittings reflect the dominance of the octahedral over the trigonal component of the crystal field, since the (0)-(1,2)-(3) and the $(0',1')$-$(2')$ splittings are much larger than the (1)-(2) and $(0')$-$(1')$ splittings. The $^2F_{7/2}$ and $^2F_{5/2}$ crystal-field energies determined here agree with those reported in an earlier study[21] except for (2) and $(2')$. A small, unexplained shift of the $(0) \rightarrow (2')$ transition to higher frequency with increasing temperature was observed. Therefore, the slight discrepancy in these energies between the two studies most likely result from the different temperatures (10 K vs 15.5 K) at which the spectra were recorded.

B. Bulk and local modes in $CsCdBr_3:Yb^{3+}$

The Raman-active first-order normal modes (corresponding to phonons near $k=0$ around the Brillouin zone center) of the $CsCdBr_3$ host can be derived from a nuclear site group analysis of the unit cell.[22,23] In the D_{6h}^4 space group of $CsCdBr_3$ with two formula units in the primitive unit cell, the Cs, Cd, and Br atoms occupy sites of D_{3h}', D_{3d}, and C_{2v}' symmetry, respectively.[24] These three sites give rise to the modes $A_{2u}+B_{1g}+E_{1u}+E_{2g}$, $A_{2u}+B_{2u}+E_{1u}+E_{2u}$, and $A_{1g}+A_{2g}+A_{2u}+B_{1g}+B_{1u}+B_{2u}+E_{1g}+2E_{1u}+2E_{2g}+E_{2u}$, respectively, with the modes $A_{2g}+2B_{1g}+B_{1u}+2B_{2u}+2E_{2u}$ being silent and $A_{2u}+E_{1u}$ being the acoustic modes.[23] From the remaining active optical modes $2A_{2u}+3E_{1u}+A_{1g}+E_{1g}+3E_{2g}$, which we refer to as bulk modes, $A_{1g}+E_{1g}+3E_{2g}$ are Raman active. All these modes are observed in the unpolarized Raman spectrum shown in Fig. 3. Both the energies and relative intensities of the Raman transitions are in agreement with previously reported Raman spectra of undoped $CsCdBr_3$.[25,26]

Pronounced vibronic sidebands are observed in both the absorption spectrum (Fig. 1) and the luminescence spectrum (Fig. 2). In the discussion below, we focus on the $(0) \rightarrow (2')$ zero-phonon line and its vibronic sideband since it is well separated in frequency from all the other transitions. The luminescence excitation spectrum of the vibronic sideband accompanying this $(0) \rightarrow (2')$ zero-phonon line (Fig. 3) reveals quite a complex structure, with many more lines spanning a wider frequency range than in the Raman spectrum. Such a pronounced qualitative difference between the Raman spectrum and the vibronic sideband is typically not observed for rare-earth-ion doped solids in which the RE^{3+} ions substitute for chemically alike ions. We do not attempt to analyze all the features of the sideband shown in Fig. 3. Rather we focus on the highest-energy transitions which are distinct and well isolated. In the isostructural compounds $CsCoCl_3$ and $CsMgCl_3$, the A_{1g} bulk mode was found to have the highest frequency of all the Raman and IR-active optical modes.[27] Also, no modes with frequency higher than the A_{1g} bulk mode were found in an analysis of vibronic sidebands in $CsCdBr_3:Co^{2+}$.[25] We therefore assume that the A_{1g} Raman transition at 162.5 cm^{-1} represents the highest-energy,

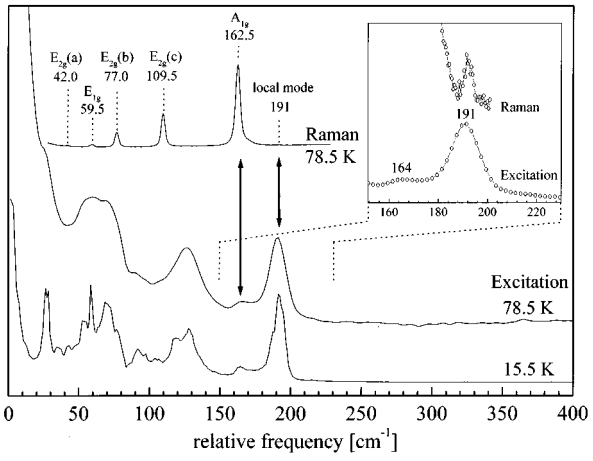

FIG. 3. Unpolarized Raman spectrum of $CsCdBr_3:Yb^{3+}$ with the incident laser wavelength at 514.5 nm (top trace) and unpolarized luminescence excitation spectra obtained by monitoring the $(0') \rightarrow (2)$ transition (Fig. 2) at 1004.5 nm (bottom traces). For the Raman and excitation spectra the frequency is normalized to the incident laser and the $(0) \rightarrow (2')$ zero-phonon line (Fig. 1), respectively. The assignments of the Raman transitions are taken from Refs. 25, 26. The inset shows an enlargement of the 180–200 cm^{-1} spectral range.

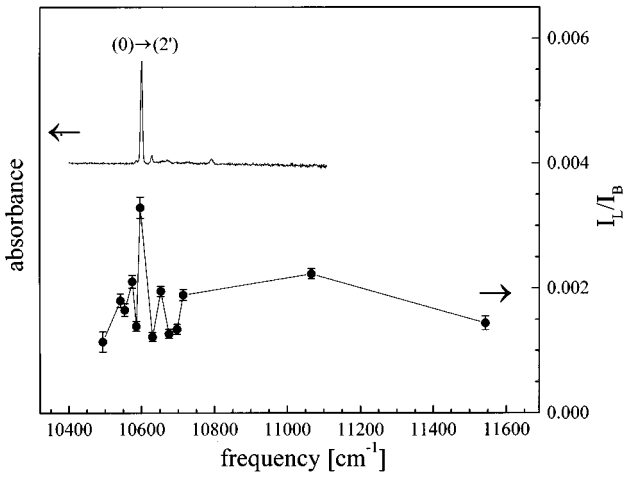

FIG. 4. Relative unpolarized Raman intensity of the bulk mode at 162.5 cm^{-1} (I_B) and the local mode at 191 cm^{-1} (I_L) as a function of the incident laser frequency in $CsCdBr_3:Yb^{3+}$ at 12 K. The enhancement of the ratio I_L/I_B on the $(0)\rightarrow(2')$ resonance is approximately a factor of 2. Part of the unpolarized absorption spectrum (from Fig. 1) is shown for comparison.

first-order bulk mode in $CsCdBr_3$. The highest-energy, first-order feature in the vibronic sideband on the other hand is observed at 191 cm^{-1}, a frequency close to the value (190 cm^{-1}) which was observed for the highest-energy mode in both $Cs_3Yb_2Br_9$ and $Cs_3Er_2Br_9$ crystals with sixfold bromide coordination.[20,28] As shown in the inset of Fig. 3, the 191 cm^{-1} mode in the vibronic sideband is also discernible as a very weak feature in the Raman spectrum. Since there are no second-order Raman transitions which could give rise to a transition at this frequency, we assign this weak Raman transition to the A_{1g} local mode associated with the $[YbBr_6]$ coordination unit. This assignment is directly confirmed by resonant Raman experiments. Figure 4 shows the Raman intensity of the 191 cm^{-1} local mode (I_L) relative to that of the 162.5 cm^{-1} bulk mode (I_B) as a function of excitation frequency and compares I_L/I_B with the unpolarized $(0)\rightarrow(2')$ absorption spectrum. The increase of I_L/I_B by approximately a factor of 2 on the $(0)\rightarrow(2')$ resonance is direct evidence that the 191 cm^{-1} mode in the Raman spectrum is due to a local mode associated with Yb^{3+}.

The relative frequencies of the A_{1g} local and the A_{1g} bulk modes can be explained on the basis of a simple model. These modes represent totally-symmetric stretching vibrations of the M–Br bond (M=Cd,Yb), with frequencies proportional in a first approximation to $\sqrt{k/\mu}$, where k is the force constant and μ is the reduced mass. Their relative frequencies should therefore be given by

$$\frac{E_{YbBr}}{E_{CdBr}}=\sqrt{\frac{k_{YbBr}\mu_{CdBr}}{k_{CdBr}\mu_{YbBr}}}. \tag{1}$$

Assuming the six M–Br bonds to be equivalent, each of the Br^- ions shares 1/6 of the charge of the metal ion in the $[MBr_6]$ coordination unit, i.e., $\frac{1}{2}$ and $\frac{1}{3}$ of an elementary charge for $[YbBr_6]$ and $[CdBr_6]$, respectively. Further assuming the force constant to be a linear function of the ionic bond strength, a ratio of $E_{YbBr}/E_{CdBr}=1.132$ is predicted from Eq. (1). This value is within 4% of the experimental ratio $191/162.5=1.175$, providing further support for the mode assignments.

The fact that the A_{1g} local-mode frequency is so similar to the respective frequency in $Cs_3Yb_2Br_9$ but significantly different from the A_{1g} bulk-mode frequency indicates a high degree of flexibility in the $[CdBr_3^-]_n$ linear chains of $CsCdBr_3$. Obviously, forces exerted by the host lattice do not constrain the $[YbBr_6]$ normal-mode frequencies to be the same as $CsCdBr_3$ bulk-mode frequencies. The Yb^{3+} defect site is apparently able to accommodate local forces by bending of adjacent metal–halogen–metal bond angles. This flexibility of the $[CdBr_3^-]_n$ linear chains is reflected not only in the large angular distribution of the crystallographic c-axis of $11\pm2°$ measured in $CsCdBr_3:Pr^{3+}$ using hole-burning Stark spectroscopy[29] but also in the fact that metal ions over a wide range of charge, size, and chemical characteristics can be doped in significant amounts into crystals of the $CsCdBr_3$ family.[24]

In Fig. 3, a weak transition in the excitation sideband at 164 cm^{-1} coincides with the strong A_{1g} bulk mode observed at 162.5 cm^{-1} in the Raman spectrum. This weak transition may be either of a vibronic or an electronic nature. Cooperative electronic transitions on the Yb^{3+} ion pairs in this material are likely and, for example, two excited Yb^{3+} ions cooperatively relaxing from their $^2F_{5/2}$ excited state in a radiative $[^2F_{5/2}(i'),^2F_{5/2}(j')]\rightarrow[^2F_{7/2}(m),^2F_{7/2}(n)]$ transition can give rise to intense green cooperative luminescence in $CsCdBr_3:Yb^{3+}$.[21] In analogy, cooperative electronic transitions of the type $[^2F_{7/2}(i),^2F_{7/2}(j)]\rightarrow[^2F_{5/2}(m'),^2F_{7/2}(n)]$ can occur in the near infrared spectral region.[20] From the energy levels calculated in Sec. II A, the transition $[^2F_{7/2}(0),^2F_{7/2}(0)]\rightarrow[^2F_{5/2}(2'),^2F_{7/2}(2)]$ is expected at 10 766 cm^{-1}, i.e., at a frequency 167 cm^{-1} above the $(0)\rightarrow(2')$ zero-phonon line. We do not have enough experimental information to assess the contribution of this electronic process to the transition intensity around 164 cm^{-1}. However, it is likely to be small, since the observation of a progression in a vibrational mode of approximately 164 cm^{-1} (see Sec. III C) indicates significant vibronic character of the 164 cm^{-1} transition. Moreover, a transition at 162 cm^{-1} was also observed in $CsCdBr_3:Pr^{3+}$, which has a different ground-state splitting.[30] Therefore, this transition arises mainly from coupling of the $(0)\rightarrow(2')$ electronic transition either to the A_{1g} bulk mode in the second coordination sphere or to an odd-parity local mode of the $[YbBr_6]$ coordination unit with a frequency similar to the A_{1g} bulk mode.

In the vibronic sideband accompanying the $^3H_4(0)\rightarrow{}^3P_0(0)$ zero-phonon line in $CsCdBr_3:Pr^{3+}$, the A_{1g} local mode of the $[PrBr_6]$ coordination unit appears at 194 cm^{-1}, and another, fairly broad vibronic transition appears at 162 cm^{-1}.[30] The slight increase of the A_{1g} local mode frequency from 191 cm^{-1} in $CsCdBr_3:Yb^{3+}$ to 194 cm^{-1} in $CsCdBr_3:Pr^{3+}$ is expected, due to the smaller mass of Pr^{3+} relative to Yb^{3+}. However the fact that the 164 cm^{-1} mode frequency in $CsCdBr_3:Yb^{3+}$ does not increase by going to

$CsCdBr_3:Pr^{3+}$ is indication for this transition not being a result of vibronic coupling to a local mode but arising from vibronic coupling of the $(0)\rightarrow(2')$ electronic transition beyond the first $[YbBr_6]$ coordination sphere to the A_{1g} bulk mode.

These results clearly show that vibronic coupling occurs almost exclusively to the local modes of the first coordination sphere with minor contributions from the second or higher coordination spheres, i.e., a characteristic vibronic interaction radius of ≈ 3 Å. In terms of electron–phonon interactions enabling non-radiative relaxation processes such as multiphonon relaxation or phonon-assisted energy transfer, this conclusion implies that most of the energy released by these processes is first transferred to the local modes of the first coordination sphere. The subsequent distribution of this vibrational energy among the various bulk modes requires resonances of those bulk modes with the local modes, a condition which may not be well satisfied for defect materials such as RE^{3+}-doped CaF_2, CdF_2, $CsMgCl_3$, or $CsCdBr_3$. Time-resolved Raman studies, such as those carried out for Cr^{4+}-doped forsterite,[31] could provide further insight into the details of the nonradiative relaxation dynamics in these materials. They might also answer the question as to whether or not the lack of any strong resonances between local and bulk modes contributes, together with the overall low frequencies of phonons in $CsCdBr_3$, to suppression of nonradiative relaxation of RE^{3+} excited states in this material.

C. Electron–phonon interaction

Two mechanisms, usually referred to as M and Δ process,[32] can mediate the interaction of the electronic and the vibrational system. The M process induces vibronic intensity through admixture of even-parity wave functions (e.g., from the $4f^{N-1}5d$ configuration) to the odd-parity $4f^N$ wave functions by coupling to an odd-parity (IR-active) vibration.[3,33–35] Such vibrationally-induced, forced electric-dipole transitions lead, for example, to vibronic transitions with a frequency differing by exactly one vibrational quantum from the zero-phonon line. The Δ or Franck–Condon process on the other hand induces vibronic intensity through slightly different equilibrium structures of electronic ground and excited states.[36] In contrast to the M process, the shift of the excited-state relative to the ground-state potential surface along one of the configurational coordinates, measured in terms of the Huang–Rhys factor S, gives rise to phonon replica in the respective mode. In the harmonic approximation, the probability of a Franck–Condon-type vibronic transition from an electronic state a and vibrational state n to an electronic state b and vibrational state m is given by

$$P_{a_n\rightarrow b_m} = P_{ab}|\langle\chi_b(m)|\chi_a(n)\rangle|^2, \tag{2}$$

where P_{ab} is the purely electronic transition probability, which is identical for all the vibrational states m and n, and $|\langle\chi_b(m)|\chi_a(n)\rangle|^2$ is the vibrational overlap integral or Franck–Condon factor, which is a measure of the electron–phonon coupling strength.[36] At zero Kelvin, the relative transition probability for the ith phonon replica, given by $P_{a_0\rightarrow b_i} = P_{ab}|\langle\chi_b(i)|\chi_a(0)\rangle|^2$, is[37]

$$\frac{P_{a_0\rightarrow b_i}}{P_{ab}} = \frac{S^i e^{-S}}{i!}. \tag{3}$$

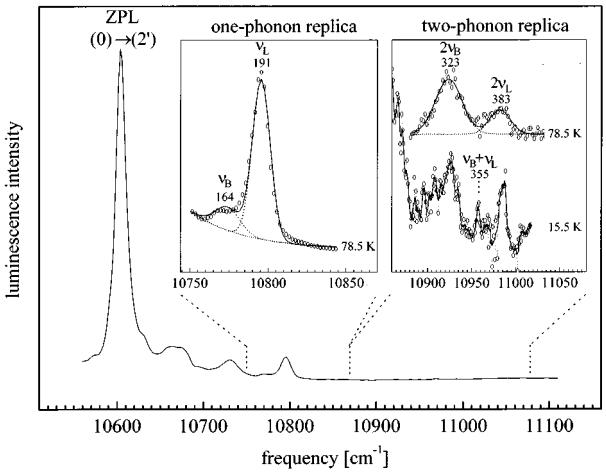

FIG. 5. Unpolarized luminescence excitation spectra of $CsCdBr_3:Yb^{3+}$. ν_B and ν_L denote the bulk-mode and local-mode frequency respectively, and the left and right insets show the one-phonon and two-phonon replica of both these modes, respectively.

Numerous studies in recent years have found that earlier assumptions that the Huang–Rhys factor is zero, implying that the M process dominates the RE^{3+}-ion vibronic intensities, were often not justified. The observation of vibronic transitions in the two-photon spectra of $SrMoO_4:Pr^{3+}$ (Ref. 38) and of two-phonon replica in $Na_5La(MO_4)_4:Pr^{3+}$ (M=Mo,W) (Ref. 39) provides direct evidence for the important role that the Δ process can play.

As shown in Fig. 5, the bulk and local modes ν_B and ν_L observed at 164 and 191 cm^{-1} in the vibronic sideband of the luminescence excitation spectrum appear as very weak two-phonon replicas at 323 and 383 cm^{-1}, respectively. That is, they appear at approximately twice their respective fundamental frequencies. This is direct evidence for a Δ process inducing the vibronic intensity. This result is consistent with selection rule considerations since both the modes ν_B and ν_L were assigned to A_{1g} modes, which as even-parity modes cannot enable M processes. The two-phonon frequencies are at ≈ 1.96 and ≈ 2.01 times the one-phonon frequencies for the modes ν_B and ν_L, respectively, indicating the highly harmonic nature of the excited-state potential surface. Note that the combination mode $\nu_B+\nu_L$ is also observed.

By using Eq. (3) it is possible, in principle, to calculate the Huang–Rhys factors S from the ratios of transition probabilities $P_{a_0\rightarrow b_1}/P_{ab}$ and $P_{a_0\rightarrow b_2}/P_{ab}$ derived from experimental transition intensities I in the luminescence excitation spectrum (Fig. 5). Under the experimental conditions used for measuring the luminescence excitation spectra, however, it is likely that the strongly absorbing zero-phonon line is partially saturated, i.e., its intensity is not proportional to

P_{ab}. Consequently, the above two ratios would be overestimated, a complication in numerous past studies.[4]

Instead, we assume that the weakly absorbing vibronic transitions are unaffected by saturation (i.e., $I \propto P$), and we only calculate the ratio $I_{a_0 \to b_2}/I_{a_0 \to b_1} = \frac{1}{2}S$ using Eq. (3) and the spectra of Fig. 5. For the modes ν_B and ν_L we then obtain $S_{\text{bulk}} = 0.15 \pm 0.03$ and $S_{\text{local}} = 0.010 \pm 0.002$, respectively. Note that $S_{\text{bulk}} > S_{\text{local}}$. This result reflects the fact that the relative intensity of the modes ν_B and ν_L in the one-phonon and two-phonon replica (Fig. 5) is reversed. Although both Huang–Rhys factors found here are within the typical range of values reported for other RE^{3+}-doped solids,[7,39] they indicate quite different electron–phonon coupling strengths of the two modes.

Whereas the configurational coordinate for the A_{1g} local mode is most likely the (average) Yb–Br bond length, the configurational coordinate describing the coupling to the bulk mode in the second coordination sphere or beyond is not directly obvious. The relatively large value of S_{bulk} indicates the occurrence of local structural changes upon excitation of the respective vibronic transitions and, on the basis of both the one-dimensional nature of $CsCdBr_3$ and the structure of the dominant Yb^{3+} pair center in $CsCdBr_3$, we can speculate on the nature of this structural rearrangement. From our results on the spatial extension of electron–phonon interactions (Sec. III B) we conclude that vibronic coupling is not only confined to within the linear chains in $CsCdBr_3$ but more specifically does not extend beyond the vibrational modes of the nearest-neighbor coordination units in the chain. With the dominant Yb^{3+} pair center being a Yb^{3+}-vacancy-Yb^{3+} arrangement, the Yb^{3+} ion therefore typically has a $[CdBr_6]$ coordination unit on one side and a [vacancy-Br_6] coordination unit on the other side along the linear chain. Since the vacancy is likely to be easily compressed, the vibronic excitation of the A_{1g} bulk mode, which involves stretching of the Cd–Br bonds, may push the Yb^{3+} ion towards the vacancy and thus induce changes in bond lengths and angles of the bromide ions linking the Yb^{3+} and the Cd^{2+} ion. The overall result of this vibronic excitation would be the introduction of coupling between local and bulk modes and a reduction of the Yb^{3+}–Yb^{3+} distance. While there is currently no experimental evidence supporting this picture, we wish to point out that EPR measurements on a sample strongly excited into the bulk-mode vibronic transition at 162.5 cm^{-1} could provide direct information on the magnitude of this structural rearrangement.[14]

IV. CONCLUSIONS

The incorporation of Yb^{3+} into $CsCdBr_3$ leads to the formation of $[YbBr_6]$ coordination units, the vibrational properties of which differ markedly from those of the host lattice. From a comparison of Raman spectra which probe host vibrations, and Yb^{3+} luminescence excitation spectra which provide a probe of local vibrations, we have shown that vibronic coupling occurs predominantly to modes of the first coordination sphere, and that vibronic contributions from the second or higher coordination sphere are weak. The spatial extent of electron–phonon interactions is estimated to be approximately 3 Å. These results all have important consequences for phonon-assisted energy transfer and multiphonon relaxation of RE^{3+} excited states. The present research has shown that vibrational energy release during relaxation of the electronic excited state of Yb^{3+} occurs through excitation first of local modes, and subsequently via energy transfer through resonances with bulk modes which complete the nonradiative relaxation process. For materials such as RE^{3+}-doped $CsCdBr_3$, where local and bulk mode frequencies differ markedly, the significant detuning of many such potential resonances undoubtedly suppresses some relaxation pathways.

ACKNOWLEDGMENTS

M.P.H. gratefully acknowledges support through a Swiss National Science Foundation fellowship. We thank Naomi Furer, Karl Krämer, and Hans U. Güdel, University of Bern, Switzerland, for growing and preparing the crystal, and Geoffrey F. Strouse, Los Alamos National Laboratory, for assistance in the resonant Raman experiments.

[1] K. H. Hellwege, Ann. Phys. **40**, 529 (1941).
[2] W. F. Krupke, Phys. Rev. **145**, 325 (1966).
[3] G. Blasse, Int. Rev. Phys. Chem. **11**, 71 (1992).
[4] G. Blasse, A. Meijerink, and C. de Mello Donegá, J. Alloys Comp. **225**, 24 (1995).
[5] L.-S. Lee, S. C. Rand, and A. L. Schawlow, Phys. Rev. B **29**, 6901 (1984).
[6] C. de Mello Donegá and G. Blasse, Chem. Phys. Lett. **183**, 367 (1991).
[7] C. de Mello Donegá, A. Meijerink, and G. Blasse, J. Phys. Condensed Matter **4**, 8889 (1992).
[8] A. Meijerink, C. de Mello Donegá, A. Ellens, J. Sytsma, and G. Blasse, J. Lumin, **58**, 26 (1994).
[9] A. Meijerink, G. Blasse, J. Sytsma, C. de Mello Donegá, and A. Ellens, Acta Phys. Pol. A **90**, 109 (1996).
[10] G. Blasse and G. J. Dirksen, J. Solid State Chem. **96**, 258 (1992).
[11] G. Meyer, Inorg. Synth. **25**, 146 (1989).
[12] D. Visser, G. C. Verschoor, and D. J. W. Ijdo, Acta Crystallogr. B **36**, 28 (1980).
[13] G. L. McPherson and L. M. Henling, Phys. Rev. B **16**, 1889 (1977).
[14] L. M. Henling and G. L. McPherson, Phys. Rev. B **16**, 4756 (1977).
[15] R. B. Barthem, R. Buisson, and R. L. Cone, J. Chem. Phys. **91**, 627 (1989).
[16] N. J. Cockroft, G. D. Jones, and R. W. G. Syme, J. Lumin. **43**, 275 (1989).
[17] J. P. Chaminade, R. M. Macfarlane, F. Ramaz, and J. C. Vial, J. Lumin. **48&49**, 531 (1991).
[18] N. J. Cockroft, G. D. Jones, and D. C. Nguyen, Phys. Rev. B **45**, 5187 (1992).
[19] F. Ramaz, R. M. Macfarlane, J. C. Vial, J. P. Chaminade, and F. Madéore, J. Lumin. **55**, 173 (1993).
[20] M. P. Hehlen and H. U. Güdel, J. Chem. Phys. **98**, 1768 (1993).
[21] Ph. Goldner, F. Pellé, D. Meichenin, and F. Auzel, J. Lumin. **71**, 137 (1997).
[22] J. P. Mathieu, *Spectres de Vibration et Symmetrie* (Herman et Cie, Paris, 1945).
[23] D. L. Rousseau, R. P. Bauman, and S. P. S. Porto, J. Raman Spectrosc. **10**, 253 (1981).
[24] G. L. McPherson and A. M. McPherson, J. Phys. Chem. Solids **41**, 495 (1980).
[25] C. W. Tomblin, G. D. Jones, and R. W. G. Syme, J. Phys. C **17**, 4345 (1984).
[26] O. Pilla, E. Cazzanelli, B. Blanzat, C. Andraud, and F. Pellé, Phys. Status Solidi B **144**, 845 (1987).
[27] G. L. McPherson and Jin Rong Chang, Inorg. Chem. **12**, 1196 (1973).
[28] M. P. Hehlen, K. Krämer, H. U. Güdel, R. A. McFarlane, and R. N. Schwartz, Phys. Rev. B **49**, 12 475 (1994).

[29] F. Ramaz, J. C. Vial, and R. M. Macfarlane, Europhys. Lett. **22**, 217 (1993).
[30] J. Neukum, N. Bodenschatz, and J. Heber, Phys. Rev. B **50**, 3536 (1994).
[31] S. G. Demos, D. M. Calistru, and R. R. Alfano, Appl. Phys. Lett. **68**, 1195 (1996).
[32] T. Miyakawa, in *Luminescence of Crystals, Molecules, and Solutions*, edited by F. Williams (Plenum, New York, 1973).
[33] T. R. Faulkner and F. S. Richardson, Mol. Phys. **35**, 1141 (1978).
[34] B. R. Judd, Phys. Scr. **21**, 543 (1980).
[35] J. Dexpert-Ghys and F. Auzel, J. Chem. Phys. **80**, 4003 (1984).
[36] B. Henderson and G. F. Imbusch, *Optical Spectroscopy of Inorganic Solids* (Clarendon, Oxford, 1989).
[37] T. Keil, Phys. Rev. **140**, A601 (1965).
[38] C. de Mello Donegá and A. Meijerink, J. Lumin. **55**, 315 (1993).
[39] C. de Mello Donegá, S. Schenker, H. F. Folkerts, A. Meijerink, and G. Blasse, J. Phys. Condensed Matter **6**, 6043 (1994).